www.czasopisma.pan.pl PAN www.journals.pan.pl
POLSKA AKADEMIA NAUK

Opto-Electronics Review 26 (2018) 149–157

Contents lists available at ScienceDirect

Opto-Electronics Review

journal homepage: http://www.journals.elsevier.com/opto-electronics review

Numerical analysis of SiGeSn/GeSn interband quantum well infrared photodetector

P. Pareek[a,b,*], M.K. Das[b], S. Kumar[b]

[a] Dept. of Electronics and Communication Engineering, Vaagdevi College of Engineering (Autonomous), Bollikunta, Warangal, Telengana, India
[b] Dept. of Electronics Engineering, Indian Institute of Technology (Indian School of Mines) Dhanbad, Dhanbad, Jharkhand, India

ARTICLE INFO

Article history:
Received 28 March 2017
Received in revised form
17 November 2017
Accepted 29 March 2018
Available online 2 May 2018

Keywords:
GeSn
QWIP
Strain balanced
Sn composition
Bandwidth
Responsivity

ABSTRACT

In this paper, detailed theoretical investigation on the frequency response and responsivity of a strain balanced SiGeSn/GeSn quantum well infrared photodetector (QWIP) is made. Rate equation and continuity equation in the well are solved simultaneously to obtain photo generated current. Quantum mechanical carrier transport like carrier capture in QW, escape of carrier from the well due to thermionic emission and tunneling are considered in this calculation. Impact of Sn composition in the GeSn well on the frequency response, bandwidth and responsivity are studied. Results show that Sn concentration in the GeSn active layer and applied bias have important role on the performance of the device. Significant bandwidth is obtained at low reverse bias voltage, e.g., 200 GHz is obtained at 0.28 V bias for a single $Ge_{0.83}Sn_{0.17}$ layer. Whereas, the maximum responsivity is of 8.6 mA/W at 0.5 V bias for the same structure. However, this can be enhanced by using MQW structure.

© 2018 Association of Polish Electrical Engineers (SEP). Published by Elsevier B.V. All rights reserved.

1. Introduction

Over the last decade, III–V based quantum well infrared photodetectors (QWIPs) transform themselves into backbone of high speed communication and sophisticated sensor systems. Also, they find their presence in ground and space-based applications such as night vision, temperature detection, early warning systems, navigation, flight control systems, weather monitoring, as well as security and surveillance [1–3]. However, their high cost and incompatibility to silicon restrict them to be used in electronic photonic integrated circuits (EPICs). EPICs offer cheap and commercially viable technology which is crucial to meet the demand of high speed communication and refined sensor systems [4,5]. Recently, a lot of research is conducted towards realizing group IV (Gr-IV) based active photosensitive devices which are cheap, as well as offer heterogeneous integration with CMOS technology to realize EPICs [6,7]. The advent of a direct band gap GeSn alloy is said to be a milestone in this quest of low cost monolithic optoelectronic devices specially photodetectors [8–10]. Add to this fact, recent progress in growth of high quality GeSn photodetectors by chemical vapour deposition (CVD), molecular beam epitaxy (MBE), and magnetron sputtering epitaxy is also motivating researchers to work towards realizing more improved versions of these detectors [11–13]. However, most of the reported works are either concentrated on telecommunication wavelength or employed bulk scale structure. So, it does not give a clear idea to understand the physics of QWIP utilizing longer wavelength range (say 3–5 μm), which is very crucial for certain applications. Therefore, modelling of GeSn QWIP is very crucial before its fabrication to study and re-engineering its properties. Particularly issues related to strain which come into play due to a large lattice mismatch between Ge and Sn. However, strain balanced structure is used to shield the active GeSn well layer from excessive strain during fabrication [14]. In a strain balanced system, strain in well region can be minimized by adjustment of a lattice constant of barrier and buffer layers. Moreover, due to its simple structure, a single quantum well structure is most appropriate for a better comprehension of various physical aspects.

In this context, authors had already proposed a model for an absorption coefficient considering interband transition in a strain balanced GeSn based single QWIP and a significant absorption in an active GeSn layer at a peak wavelength of 3.34 μm is obtained [15]. However, absorption coefficient is not the sole performance parameter for a QWIP, but a large bandwidth and high responsivity are necessary ingredients of a competent detector. Therefore, a detailed analysis for frequency response and responsivity in GeSn based QWIP is necessary. This analysis requires understanding the physical phenomena like capture of carriers into quantum well,

* Corresponding author.
E-mail address: ppareek1@gmail.com (P. Pareek).

https://doi.org/10.1016/j.opelre.2018.03.002
1896-3757/© 2018 Association of Polish Electrical Engineers (SEP). Published by Elsevier B.V. All rights reserved.

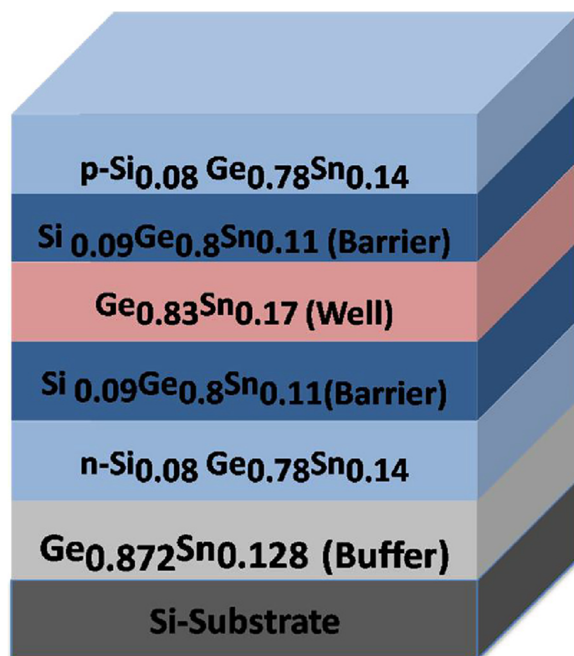

Fig. 1. Schematic structure of strain balanced GeSn QWIP (not to scale).

escape of carriers from quantum well, and effect of barrier height on these phenomenon. Although these aspects have been studied in depth by numerous theoretical and experimental investigations in case of conventional III–V based QWIPs [16–19]. But, physics considering all the above mentioned aspects is not clearly understood completely in case of Gr-IV based interband QWIPs. Even though few studies to demonstrate GeSn based p-i-n detectors using quantum well structure have been reported in Refs. [20,21], theoretical modelling for the device, considering the quantum mechanical transport, has not been reported yet. Also, the effect of Sn content on the performance of the device has not been explored in detail to the best of author's knowledge.

In the present paper, we have studied the frequency response and responsivity of a strain balanced $Si_{0.09}Ge_{0.8}$ $Sn_{0.11}/Ge_{0.83}Sn_{0.17}$ QWIP by varying different material parameters, Sn-composition in particular. Interband transition is considered in this analysis which yields a peak wavelength of operation in the range of 2.9-3.86 μm (effective bandgap ~0.3–0.42 eV). It may be relevant to mention here that the present analysis is done at room temperature, i.e., 300 K. However, the performance parameters of the proposed QWIP will be more superior at 77 K which is the operating temperature of conventional QWIPs. At the same time it is crucial and demanding to optimize the performance of a group IV QWIP at 300 K. As most of the significant applications of integrable Group IV based QWIPs require room temperature operation [22].

The paper is organized as follows. In Sect. 2 a brief model description is explained along with its design considerations. Sects. 3 & 4 give the detailed derivation of frequency dependent photogenerated current density and responsivity, respectively. Sect. 5 gives results and their discussions. Finally, summary of the work with conclusion is provided in Sect. 6.

2. Model description

A single quantum well with double barrier is considered here due to its simple structure and hence for better understanding of the aspects responsible for QWIP operation. The schematic structure of the device is shown in Fig. 1. Structure consists of $Ge_{0.83}Sn_{0.17}$ quantum well layer sandwiched between two wide bandgap $Si_{0.09}Ge_{0.8}$ $Sn_{0.11}$ barriers. The Ge and Sn content of well and barriers are optimized to facilitate a low direct bandgap well layer, as well as a wide bandgap barrier for quantum carrier confinement [15]. The thickness of well is chosen as 76 Å to enable single bound state. This thickness of well is also above the critical thickness to prevent dislocations.

Both quantum well and barrier are considered to be undoped in this case. This double barrier quantum well is considered to be grown on a relaxed $Ge_{0.872}$ $Sn_{0.128}$ buffer to form a strain balanced structure. The Ge and Sn content of the buffer layer is chosen such that the strain induced by buffer on well and barriers are exactly the same but opposite in nature. Thus, quantum well is compressively strained and barrier layers are tensile strained with respect to a buffer layer in order to ensure the strain balance condition. According to strain balance condition [23], the barrier thickness is computed as 35 Å. But this small dimension may lead to a very high electric field across depletion region which may cause breakdown of the device. Thus, this fact is considered while choosing the dimension of barrier thickness. As a result, barrier thickness is increased by 35% so that the structure still remains under partial strain balance conditions. Hence, the thickness of the barrier is taken as 50 Å. Now, this partial strain balanced structure is further sandwiched between two heavily doped contact layers (p-$Si_{0.08}$ $Ge_{0.78}$ $Sn_{0.14}$ and n-$Si_{0.08}$ $Ge_{0.78}$ $Sn_{0.14}$) to form a p-i-n structure. TE polarized light is assumed to be incident from top as shown in Fig. 1. Moreover, the fabrication of the proposed model is quite feasible owing to the recent progress in fabrication of GeSn based devices. For instance, Ghetmiri et. al. reported the fabrication of similar type of strain balanced, SiGeSn/GeSn/SiGeSn quantum well structure in 2017 [24]. The same group also reported the fabrication of a 8.2 nm thick GeSn quantum well layer in 2016 [25].

In this work, intersubband transition is not considered due to the following reasons. Firstly, the thickness of quantum well is chosen such that single bound energy state [in conduction band, heavy hole (HH) band and light hole (LH) band each] exists in the well. Secondly, the intersubband transition is difficult to take place due to consideration of normal incidence of light in this model. As intersubband absorption in quantum well occurs when polarization of the incident radiation has a component along the growth direction. Here, the quantum well is assumed to be grown vertically (z-direction). Hence, the incident light needs to have a polarization component along z-direction to satisfy the polarization selection rule. Thus, the incident radiation, normal to the quantum well plane, has zero absorption probability. Whereas, for interband transitions, it states that only transitions involving same quantum number states in the valence and conduction bands are allowed which is considered in this work, i.e., ($E_{HH1} \rightarrow E_{c1}$) transition. Now, there may be a little chance of E_{LH1}-E_{HH1} intersubband transition. But, this can easily be neglected due to a very low band offset of LH band as reported by the authors previously [15]. It causes confinement of light holes weaker which become worse on increasing electric field further. Hence, only interband transition is considered this work.

3. Frequency response

In this section, a detailed carrier transport mechanism is considered while obtaining expression of frequency dependent current density in QWIP. The calculation is carried out for a generalized distribution of carriers generated by a light impulse, in the active quantum well layer. Let the light of an appropriate wavelength be incident on p-side of the device as shown in Fig. 2, where w_d is the thickness of the active QW layer. As shown in figure, position coordinate, x is pointed from n to p. For the sake of simplifing the

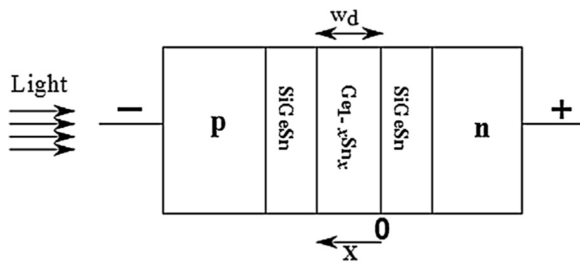

Fig. 2. Schematic of strain balanced GeSn QWIP.

solution, we consider the time dependent approach in this calculation.

This can be done by replacing x with an appropriate time dependent expression as reported by Das and Deen [26]. Further, in this study the barriers and quantum well are assumed to be undoped and unintentional doping is also assumed to be negligible. Also, bias voltage is assumed to be large enough so that carriers move with saturation velocity throughout the device. On incident of light, electron hole pairs (EHPs) are generated and the generated carriers within the active layer, electrons and holes move in opposite directions under influence of electric field. Diffusion of photogenerated carriers can be neglected due to fully depleted active layer. Let us first take the case of moving electrons. Current density due to moving electrons is denoted by J_{em}. Actually, J_{em} depends upon the distribution function of uncollected electrons in the active region of the device [26]. The distribution function represents uncollected electrons per unit volume and also includes the effect of exponential decaying nature of light intensity. So, from Fig. 2, expression of current density, J_{em} produced due to light impulse incident under low level of illumination at time't', can be expressed as:

$$J_{em} = Kqv_e\left[1 - \exp(-\alpha(w_d - v_e t)\right], \quad (1)$$

where K is the constant which depends upon the intensity of input light, v_e is the saturation velocity of electrons and α is the absorption coefficient in the active region. Absorption coefficient of active $Ge_{0.83}Sn_{0.17}$ layer is computed by calculating the bound energy states and transition probabilities by finite difference method as reported in our previous work [15]. Saturation velocity of carriers in GeSn alloy has not reported in any literature and we have used Ge saturation velocity in this calculation [27].

Now, because of heterojunctions, band discontinuities at well barrier interfaces are produced. The moving electrons are captured in a potential well created by these band discontinuities. Figure 3 shows simple depiction of carrier transport mechanism in a single quantum well under bias and can be explained as follows.

The thickness of the well is chosen such that the ground state in a conduction band is very near to top of the well, i.e., *i.e.* continuum. This means that the probability of carriers to escape from conduction band to continuum state is more likely by thermionic emission as shown in Fig. 3. Moreover, at temperature above 45 K, classical thermionic process is the dominant process of charge transport in QWIP as suggested by Bandara and Gunapala [28]. Therefore, we have considered classical thermionic emission process in this study. Thermionic emission is a slow process which depends upon the temperature and bias dependent barrier height. The thermal escape rate can be represented in terms of voltage dependent band offset as [29]:

$$r_{esc} = \frac{1}{w_d}\sqrt{\frac{K_B T}{2\pi m_c}}.e^{\left(\frac{-E_c}{K_B T}\right)} \quad (2)$$

where r_{esc} is the thermionic emission rate, K_B is the Boltzmann constant, T is the temperature in Kelvin, E_c is the effective barrier height of conduction band (valence band in case of hole) and m_c

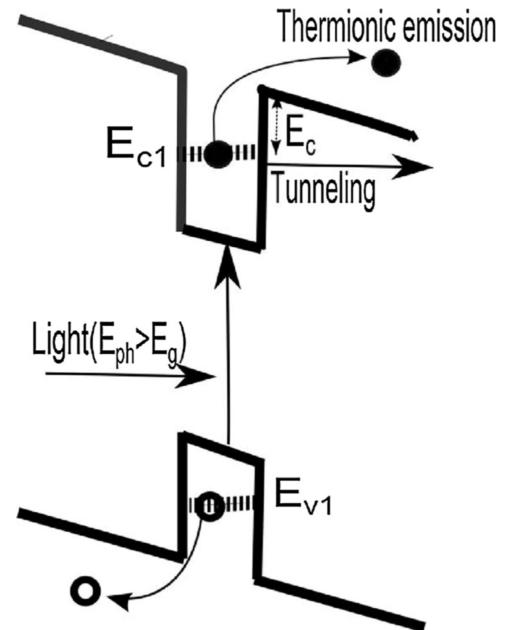

Fig. 3. Basic processes of carrier transport mechanism in Single QWIP; where E_c is the effective barrier height for conduction band, E_{c1} and E_{v1} are the bound states in conduction band and valence band, respectively.

is the effective mass of electrons in Γ valley conduction band of a GeSn well. Effective barrier height represents the change in the intrinsic bandoffset due to electric field. The band offset for conduction band considering strain is computed with the help of Van de Walle's model solid theory [30] in our previous work [15]. After calculation of band offsets effective barrier height is calculated with the help of a simple approximation as reported by Das and Das [31].

Another emission process which is not insignificant in the present case due to thin barriers, is tunneling. Tunneling occurs when carriers succeeded to get through the thin barrier layers as shown in Fig. 3. The tunneling escape rate for electrons can be expressed as [32]:

$$r_{tunnel} = \left(\frac{\pi\hbar}{2m_c w_d^2}\right).\exp\left(-\frac{2L_b E_c}{\hbar}\right) \quad (3)$$

where L_b is the barrier thickness, E_c is the effective barrier height of conduction band, m_c is the effective mass of electrons in Γ valley conduction band of GeSn well, $\hbar$ is the reduced Planck's constant.

Thus, electrons in the well can be escaped by two mechanisms namely thermionic emission and tunneling. Apart from escape, electrons in quantum well may also recombine with holes. The recombination is governed by life time of electrons. In literature, no exact value of life time of electrons for direct band gap GeSn alloy has been reported to the best of our knowledge. Moreover, the standard method of time-resolved photoluminescence (TRPL) is not well-suited to the study of GeSn alloys. Thus, the study of recombination lifetimes in GeSn alloys is of paramount importance to the actualization of GeSn based optoelectronic devices. Researchers have so far succeeded in measurement of life time in low Sn content GeSn layer. For instance 5 ns is reported in Sn content of 2% in a GeSn thin layer by Arizona State University researchers [33].

Though, in the present case escape rates are expected to be more dominant than that of recombination rate due to small band offsets. Also, Sn concentration is much higher which enhanced band to band recombination, so we have used recombination life time approximately as 10 ps which is even lesser than that of III–V materials.

Now, the number of electrons in quantum well gets reduced by thermionic emission, tunneling and recombination.

So, considering both, thermionic emission and tunneling, the rate equation for electrons in conduction band can be written as:

$$\frac{\partial n_{QW}}{\partial t} = \frac{J_{em}}{q} - n_{QW}R_e \tag{4}$$

where,

n_{QW} is the electron sheet concentration in quantum well.

J_{em} is the Current density at quantum well due to moving carriers.

$r_{e,esc}$ is the rate of thermionic emission of electrons from quantum well.

$r_{e,r}$ is the rate of recombination of electrons in quantum well.

$r_{e,tunneling}$ is the rate of tunneling of electrons from quantum well.

$R_e = r_{e,esc} + r_{e,r} + {}_{e,tunneling}$ i.e. total rate.

$v_e =$ is the saturation velocity of electron.

As the well is undoped, we simply calculate n_{QW} by a relationship as reported in Ref. [34]. Now, the rate equation in quantum well using the expression of J_{em} is written as:

$$\frac{\partial n_{QW}}{\partial t} = K.v_e\,(1\text{-}\exp(\text{-}\alpha\,(w_d\text{-}v_e t))\text{-}\,n_{QW}R_e \tag{5}$$

After solving this linear differential equation with appropriate boundary condition (i.e., at t = 0; $n_{QW} = 0$), expression for n_{QW} is obtained as:

$$n_{QW}(t) = K.v_e\left[\frac{1}{R_e} - \frac{1\text{-}\exp(\text{-}\alpha w_d)}{(\alpha v_e\text{+}R_e)}\right].[\exp(\alpha v_e t)\text{-}\exp(\text{-}R_e t)] \tag{6}$$

Let the electron concentration over the quantum well, i.e., in continuum state is n(t), which can be expressed in term of electron sheet concentration in quantum well as [35]:

$$n(t) = n_{QW}(t)\frac{R_e}{v_e} \tag{7}$$

Again n(t) can be written by substituting n_{QW} (t) from above expression:

$$n(t) = K.\left[\frac{1-\exp(\text{-}\,\alpha w_d)}{\left(\frac{\alpha v_e}{R_e}+1\right)}\right]\exp[(\alpha v_e - R_e)t] \tag{8}$$

Taking Laplace transform of the above expression, frequency dependent electron concentration can be expressed as:

$$n(j\omega) = K.\left[\left(\frac{1-\exp(-\alpha w_d)}{\left(\frac{\alpha v_e}{R_e}+1\right)}\right)\cdot\left(\frac{1}{\alpha v_e - R_e - j\omega}\right)\right] \tag{9}$$

The similar calculation is repeated in case of hole in the valence band. Let current density due to moving holes is J_{hm}. It depends on photogenerated uncollected holes and is expressed as:

$$J_{hm} = K.q.v_h.\,[\exp(\text{-}\alpha v_h t)\text{-}\exp(\text{-}\alpha w_d)] \tag{10}$$

Similarly for holes, frequency dependent hole density can be obtained as:

$$p(j\omega) = K.R_h\left[\frac{1}{(R_h-\alpha v_h)(\alpha v_h + j\omega)} - \frac{\exp(-\alpha w_d)}{(j\omega)(R_h + j\omega)}\right] \tag{11}$$

where v_h is the hole saturation velocity and R_h is the total rate of recombination and escape for holes.

Finally, the frequency dependent current density can be written as:

$$J(s) = n(s)qv_e + p(s)qv_h \tag{12}$$

K is the constant part of the generalized distribution function of uncollected electron hole pairs per unit volume and is expressed as [26]:

$$K = \frac{P_i\alpha}{AE_p} \tag{13}$$

where P_i is the input optical power, A is the area of cross section, E_p is the photon energy and α is the absorption coefficient of active region. Area of cross section is taken as 60 μm^2 considering V number of the fiber at peak wavelength [36,37]. Input optical power is taken as 10 mW.

4. Responsivity calculation

Besides frequency response, responsivity is very crucial performance parameter for a detector. It is defined as the ratio of dc photocurrent to the incident optical power [37]. If the responsivity is too small for a detector, then a high bandwidth will be futile. In order to calculate responsivity, photocurrent density needs to be calculated first. For this, continuity equation and rate equation should be solved simultaneously under dc conditions.

Firstly, let us take the case of electrons in a conduction band. Rate equation in quantum well for electrons can be written in a similar manner as mentioned in Sect. 2. However, in this case time dependent generation rate is not required to incorporate in current density and, thus, written separately. So, both the equations are analogous to each other.

Now, the rate equation in quantum well for electrons assuming capture probability of electrons in well as unity, can be written as:

$$\frac{dn_{QW}}{dt} = \frac{J_i}{q} + G(x,t).w_d - n_{QW}.R_e \tag{14}$$

$$G(x,t) = \alpha I_0\exp(-\alpha x) \tag{15}$$

where,

n_{QW} is the sheet concentration of electrons in quantum well.

R is the total rate of escape and recombination for electrons,

G(x,t) is the generation rate of carriers in continuum state, I_0 is the intensity of incident light and α is the absorption coefficient of active layer,

J_i is the injected current density due to electrons in quantum well.

At steady state $\frac{dn_{QW}}{dt} = 0$

$$J_i = (I_0\alpha\exp((-\alpha x).w_d - n_{QW}.R_e).q \tag{16}$$

As carriers are moving with saturation velocity throughout the device, the diffusion current is assumed to be negligible. Now, the continuity equation over quantum well, considering this assumption can be written as:

$$\frac{\partial n}{\partial t} = -\frac{n-n_0}{\tau} + v_e\frac{\partial n}{\partial x} \tag{17}$$

where τ is the recombination life time of electrons, n_0 denotes the equilibrium concentration of electrons, v_e is the saturation velocity of electron. Further on neglecting n_0.

At steady state $\frac{\partial n}{\partial t} = 0$

$$n(x) = C.\exp\left(\frac{x}{\tau v_e}\right) \tag{18}$$

Applying boundary conditions:

At x = 0 from Fig. 2, electron concentration is given by:

$$n(0) = \frac{J_i}{qv_e} \tag{19}$$

Thus, the position dependent electron density is given by:

$$n(x) = \frac{I_0.\alpha\exp(-\alpha x).w_d - n_{QW}.R_e}{v_e}.\exp\left(\frac{x}{\tau v_e}\right) \tag{20}$$

Table 1
Material parameters for Si, Ge and α-Sn at 300 K, used in our calculations; a = lattice constant in Å [38], C_{11},C_{12} = elastic stiffness coefficient in GPa [39], $m_{c\Gamma}$ is effective mass at Γ valley of conduction band (m_0) [38]; $E_{v,av}$ = valence band average energy in eV [30]; b,a_c,a_v,a_L = deformation potential in eV [39]; γ_1, γ_2 = Kohn Luttinger parameters [38]; n_r = refractive index [23]; ∇_0 = spin- orbit splitting in eV [30].

Material	a	$m_{c\Gamma}$	C_{11}	C_{12}	∇_0	b	a_c	a_v	a_L	γ1	γ2	n_r
Si	5.4307	0.528	165.77	63.93	0.04	-2.1	1.98	2.46	-0.66	4.22	0.39	3.434
Ge	5.6573	0.038	128.53	48.26	0.30	-2.9	-8.24	1.24	-1.54	13.38	4.24	4.051
α-Sn	6.4892	0.058	69	29.30	0.80	-2.7	-5.33	1.58	-2.14	-15	-11.45	5.791

Table 2
Calculated energy bandgap (E_g), band discontinuities (ΔE_c, ΔE_v), Eigen energy states (E_{c1}, E_{v1}) and effective energy band gap ($E_{g,effective}$) in QWIP, for different Sn composition (*x*) in active quantum well.

x	E_g (eV)	ΔE_c (eV)	ΔE_v (eV)	E_{c1}(eV)	E_{v1}(eV)	$E_{g,effective}$
0.15	0.3727	0.1062	0.1173	0.0375	-0.0120	0.4222
0.17	0.3223	0.112	0.1438	0.0370	- 0.0117	0.371
0.19	0.2734	0.1153	0.1704	0.0113	-0.0364	0.3211

The electron density in a total active region is obtained by the averaging n(x) over the total thickness; w_d. After integrating, n is obtained as:

$$n = \frac{1}{w_d}\left[\frac{I_0.\alpha.\, w_d\left[\exp\left(w_d\left(\frac{1}{\tau v_e}-\alpha\right)-1\right)\right]}{v_e\left(\frac{1}{\tau v_e}-\alpha\right)} - \frac{n_{QW}R_e(1-\exp(\frac{w_d}{\tau v_e}))}{v_e(\frac{1}{\tau v_e})}\right] \quad (21)$$

Thus, the current density due to electrons, i.e., J_n can be obtained from the above expression

Similar expression can be derived for holes in valence band of quantum well. Current density for holes in the valence band, J_p can be written as:

$$J_p = \frac{q}{w_d}\left[\frac{I_0.\alpha w_d.[\exp(-w_d(\alpha+\frac{1}{\tau v_h})-1)]}{(\alpha+\frac{1}{\tau v_h})} - \frac{P_{QW}.R_h(1-\exp(\frac{-w_d}{\tau v_h}))}{(\frac{1}{\tau v_h})}\right] \quad (22)$$

where v_h is hole saturation velocity, P_{QW} is hole sheet concentration in quantum well. Responsivity, R can be obtained with help of following expression.

$$R = \frac{(J_n + J_p)}{P_i}A \quad (23)$$

where A is area and P_i is input optical power.

5. Results and discussion

Material parameters of SiGeSn and GeSn, required for calculation photocurrent density, are not readily available in literature. Linear interpolation technique is used to calculate the parameters like lattice constant, elastic constants etc. using the values those parameters for Si, Ge and Sn materials. Energy band gap for GeSn and SiGeSn are also calculated using the linear interpolation but considering bowing parameters [23]. Band discontinuities in conduction band (ΔE_c) and valence band (ΔE_v) are calculated by using model solid theory considering the strain balanced condition. The values of important material parameters used in the calculation are summarized in Table 1 for quick reference. Now using ΔE_c and ΔE_v, Eigen energy states are obtained in conduction band (E_{c1}) and valence band (E_{v1}) by solving Schrödinger equation for quantum well [15]. After calculating E_g, E_{c1} and E_{v1}, the effective band gap. i.e., ($E_{c1} - E_{v1} + E_g$) is estimated for direct interband transition in QWIP assuming top of the valence band as refrence level of zero value. Calculated values of E_g, ΔE_c, ΔE_v, E_{c1}, E_{v1} and effective band gap ($E_{g,effective}$) for different Sn compositions (say, *x*) in the well are listed in Table 2. It is clear from the table that, as *x* increases, E_g decreases. Moreover, lattice mismatch between constituent layers of QWIP increases considerably. The feasibility of such narrow band gap lattice missmatched Ge_{1-x} Sn_x material fabrication is demonstrated by several researchers in recent times [40–42,24,25]. It is clear from values of $E_{g,effective}$, the range of operational wavelengths for the proposed QWIP spans from 2.9-3.86 μm. It may be relevant to mention that transition from heavy hole valence band (HHVB) is considered in our analysis as it is supported by the TE mode.

Further, for some material parameters like saturation velocity of carriers in Sn is not available. In that case, value for Ge is approximated to the value for GeSn alloy as the Sn composition in the alloy is low. After these calculations, absorption coefficient, α for dominant HHVB – Γ-valley conduction band(CB) direct transition in QWIP is calculated by obtaining transition rate as reported by the authors earlier [15].

Validation of any theoretical model based on experimental data is always important. But no experimental results for the same structure, proposed here, is available in literature till now, to the best of our knowledge. However, we tried to verify our model by comparing the measured responsivity value for similar structure as reported by Cong et. al. very recently [43] in the following way. In the structure proposed by Cong et al., maximum responsivity is obtained as 93 mA/W (say R_{expt}) for active layer thickness (say d_{expt}) of 300 nm whereas the active layer thickness in the proposed structure (say d_{model}) is 7.6 nm. Now, the measured value of responsivity corresponds to the active layer thickness of 7.6 nm can be approximated as:

$$\begin{aligned} R &\approx \{1-\exp(-\alpha_{model}d_{model})\}/\{1-\exp(-\alpha_{expt}d_{expt})\}R_{expt} \\ &\approx (\alpha_{model}d_{model}/\alpha_{expt}d_{expt})R_{expt} \end{aligned} \quad (24)$$

In this approximation we have neglected the diffusion current component. If the absorption coefficient in active layers, α_{expt} and α_{model}, respectively for experimental and proposed structure, is taken same, the value of R becomes 2.35 mA/W whereas we have obtained 8.6 mA/W from our model. Though these values are close but the obtained value from our model is higher than the calculated value using above approximated equation. This may be due to the consideration of same absorption coefficient for active layers in the proposed and experimental structure. The active GeSn layer in the experimental structure is bulk type and less direct band gap in nature (Sn content is of 0.08) whereas, it is QW and of more direct band gap nature (Sn content is of 0.17) in the proposed structure. So, the direct band gap nature of the $Ge_{0.83}$ $Sn_{0.17}$ layer, as well as quantum mechanical characteristics gives a higher absorption coefficient than that in bulk and indirect active layer considered in Ref. [43]. If we would use $\alpha_{model} > \alpha_{expt}$, the values would be closer.

From the theoretical analysis in previous two sections, it is expected that the Sn-composition in GeSn well and applied bias have important role on the performance of SiGeSn/GeSn/SiGeSn QWIP. In this section performance of the device is analyzed by varying both Sn-composition and bias.

To understand the effect of Sn content first, frequency response of the device is computed using Eq. (12) for frequency dependent current density derived in Sect. 2. Normalized frequency response of the device for different Sn compositions but at a particular bias are plotted in Fig. 4(a). In this analysis, we consider Sn content in well to be varying from 0.15 to 0.2. After 20% of Sn concentration, it becomes difficult to fabricate GeSn layer due to restriction of critical thickness [44]. It is clearly observed from the plot that with increasing Sn content in quantum well layer, a 3-dB bandwidth increases.

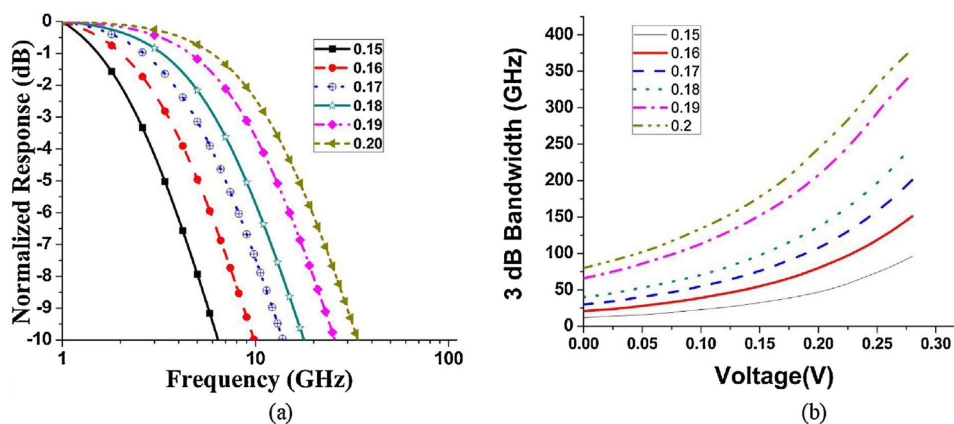

Fig. 4. (a) Plot of frequency response for GeSn quantum well for different Sn conent at zero bias; 4 (b) Plot of 3 dB bandwidth as a function of applied bias for different Sn content.

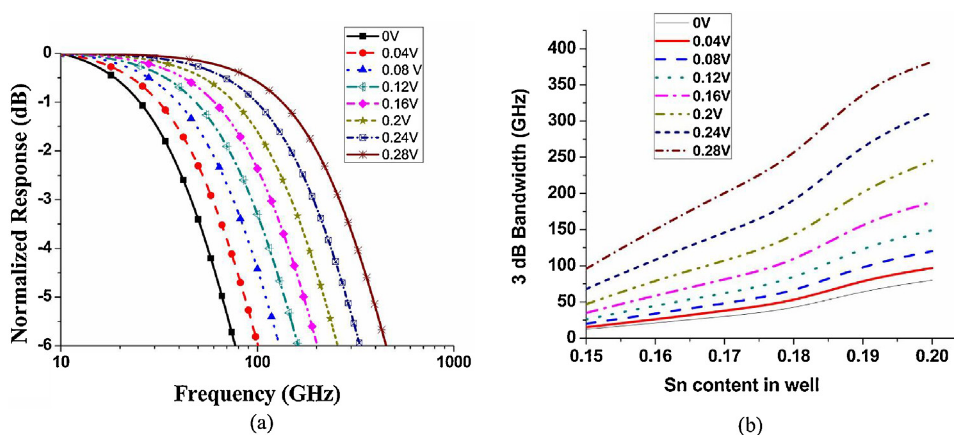

Fig. 5. (a). Plot of frequency response for $Ge_{0.83}$ $Sn_{0.17}$ quantum well for different biases; (b) Plot of 3 dB bandwidth as a function of Sn content for different applied bias.

But, the variation of 3-dB bandwidth is not linear. To understand the variation clearly, a plot of a 3-dB bandwidth with bias voltage for different Sn content is shown in Fig. 4(b). It is seen that the variation of a 3-dB bandwidth with Sn-composition is nonlinear which is due to the combined effect of barrier width reduction and Sn-content dependent escape rate of carriers. Actually, in the present model, authors have considered strain balanced structure concerning the ease of fabrication and to avoid any dislocation in active layer due to excessive strain. Strain balanced structure is ensured by selecting the Sn content in the active layer and barrier width such that strains observed by active well and barrier w.r.t. buffer, are equal and opposite in nature. Thus, in accordance with the increment of Sn content, width of barrier is reduced to maintain the strain balance condition. As the barrier width decreases, electric field increases and the effective barrier height for carriers in the well decreases and hence, both the tunneling and thermionic escape rate of carrier increase. Again, with increasing Sn content in the well, effective barrier heights increases and thus escape rate decreases. But the effect of barrier width decrement is dominant here. So, the bandwidth increases from ~50 GHz to ~400 GHz due to faster removal of photogenerated carriers. It is also seen from this plot that at high bias, nature of variation in bandwidth remains almost same but its value is enhanced. Effect of bias on the performance of the device can be observed from Fig. 5(a) where, the frequency response is plotted for different values of applied bias. It is clear from the figure that the transit time limited 3-dB bandwidth increases nonlinearly with bias.

It may be mentioned here that the maximum bias is not set too high to limit the electric field and hence to prevent breakdown in the active region. However, the variation of a 3-dB bandwidth with Sn composition for different bias voltages is shown in Fig. 5(b) for better understanding of bias dependence. For full range of Sn-content bandwidth increases with bias. The reason behind this variation can be explained as follows. On increasing applied bias, effective barrier height at particular Sn-content reduces which causes exponential increase in rate of thermionic emission of carriers from the well. The enhancement in emission rate with reduced barrier height can be explained from Eq. (2). This causes faster removal of carriers from the well and as a result, transit time reduces. The increment in a bandwidth becomes more prominent as bias increases. At high bias, escape of carriers increases rapidly by both thermionic emission and tunneling due to increase in electric field. However, due to the consideration of room temperature (300 K) operation of QWIP, thermionic emission of carriers dominates the tunneling process. Thus, an optimization should be made for the appropriate values of Sn-content considering critical thickness and bias concerning electric field and requirement of type of quantum well. In literature, large bandwidths for GeSn, as well as Ge photodetectors are experimentally reported [45–47], which are approximately in the range of bandwidth values as obtained from our calculation.

Responsivity is another important performance parameter of a QWIP. Responsivity is calculated using Eq. (23) and is plotted as a function of bias in Fig. 6 for three different values of Sn-content.

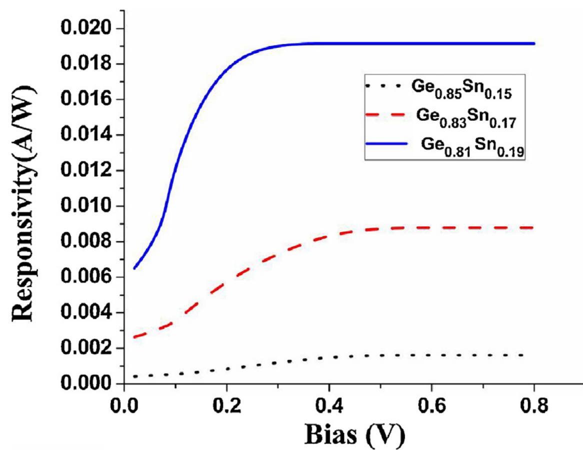

Fig. 6. Plot of responsivity as a function of bias for different Sn contents.

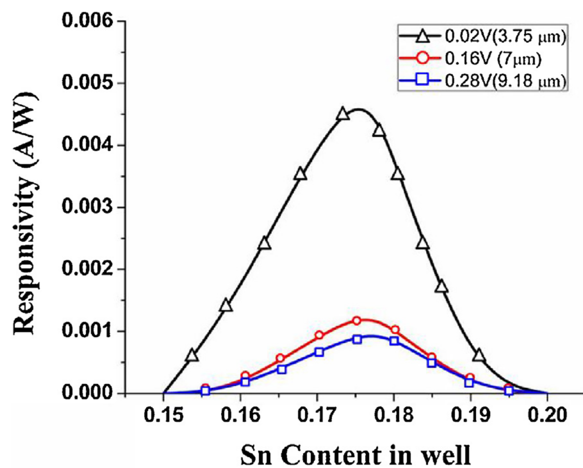

Fig. 7. Plot of responsivity as a function of Sn content for different Bias.

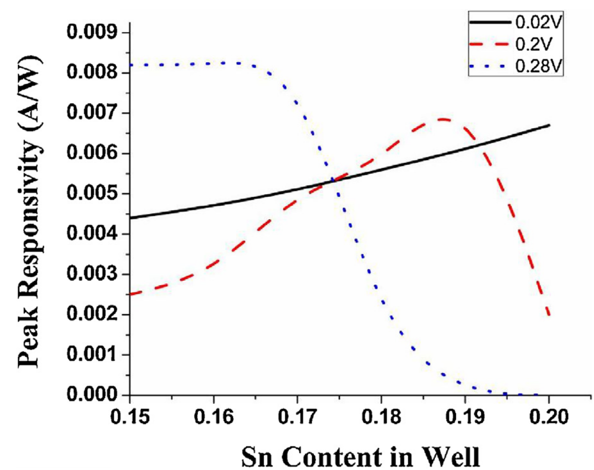

Fig. 8. Plot of peak responsivity vs. Sn content in well for different bias.

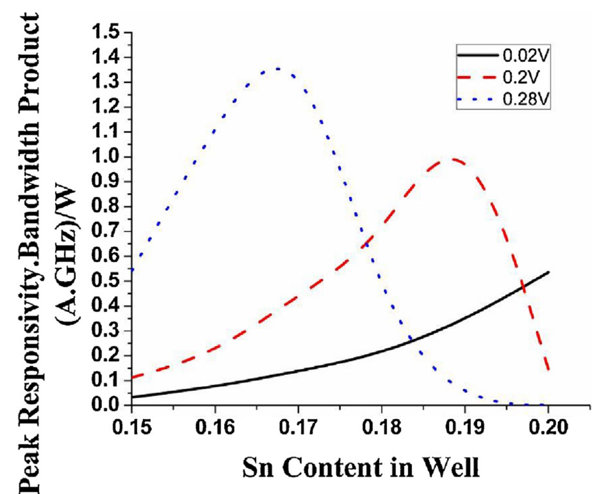

Fig. 9. Plot of peak responsivity-bandwidth product vs. Sn content in well for different bias.

It may be mentioned here that, as Sn-content increases the peak absorption coefficient (α_{peak}) increases and corresponding absorption wavelength also shifts towards longer wavelengths as reported by the authors elsewhere [15].

In this plot, the peak absorption coefficient is taken for a particular value of Sn-content (x), for example, α at wavelength of 3.5 μm which is a peak wavelength corresponding to $x = 0.17$ is considered [15]. However, shift in peak absorption wavelength with bias is not considered in this plot. It can be clearly observed from the figure that responsivity initially increases with bias and after a particular value of bias it saturates. This is due to the enhancement of electric field with the bias. As the electric field increases, the effective barrier height reduces and thus confinement of carriers in the well also decreases.

As a result, recombination of the carriers decreases which ultimately led to increase in current and hence responsivity. Saturation in responsivity is due to the saturation velocity of the carriers. A maximum responsivity of 8.6 mA/W is obtained at reverse bias of 0.5 V. This result is in approximate agreement with recently published article which reports 93 mA/W responsivity for a 300 nm thick active GeSn layer [43]. It is also seen from the figure that saturation value of responsivity increases with x but its nature of variation remains same. But, saturation starts at lower value of bias for high value of x. To study the effect of Sn-content on the responsivity, its variation with Sn content is shown in Fig. 7.

In this plot three different bias voltages are considered and operating wavelengths are kept fixed at three different values which are nothing but peak absorption wavelengths corresponds to the respective bias voltages for a constant x (mid way of the whole range of variation in x). It is very interesting to observe that maximum responsivity decreases sharply at high bias. As the bias voltage increases, absorption coefficient decreases abruptly due to poor confinement of carriers in the well [15].

Another aspect is to study the effect of x on peak responsivity. This can be obtained by calculating current based on the peak absorption coefficient, i.e., by choosing peak absorption wavelength for each x. Plot of peak responsivity as a function of x for different bias voltages is shown in Fig. 8. It is interesting to observe that responsivity increases almost linearly with x for low value of bias. But, it initially increases and after a particular x, decreases for high value of bias say, 0.2 V, 0.28 V etc. Variation in responsivity with x is mainly due to the increase of absorption in GeSn layer with x [48]. Absorption coefficient mainly depends on the probability of transition between energy states and position of these states depends on the effective barrier height. Barrier height is varying with both bias and Sn-composition in this plot. However, at low bias, effect of x on barrier height is insignificant where as the effect at high bias is significant. Thus, the nature of variation in peak responsivity with x at high bias differs from the variation at low bias.

Low responsivity as obtained here, can be increased by employing multiple quantum well structure. But, in that case, transit time

Table 3
Some important performance parameters of SiGeSn/GeSn QWIP for different Sn contents and applied bias.

Bias (V)	x = 0.15			x = 0.17			x = 0.19		
	BW (GHz)	R_p (A/W)	R_p.BW (A.GHZ/W)	BW (GHz)	R_p (A/W)	R_p.BW (A.GHZ/W)	BW (GHz)	R_p (A/W)	R_p.BW (A.GHZ/W)
0.02	5.5	0.00432	0.02376	23	0.0051	0.01173	54	0.006	0.324
0.04	10	0.0046	0.046	30	0.0052	0.156	67	0.0062	0.4154
0.08	14	0.0048	0.067	40	0.0054	0.216	85	0.0064	0.544
0.12	21	0.0051	0.1071	54	0.0056	0.3024	108	0.0066	0.7128
0.16	31	0.0041	0.1271	73	0.0058	0.4234	138	0.0069	0.9522
0.2	45	0.0025	0.1125	99	0.0045	0.4455	179	0.0065	1.1635
0.24	66	0.0079	0.5214	150	0.0080	1.2	237	0.00001	0.0023

will increase which will reduce the bandwidth of the device. So, the product of peak responsivity and bandwidth is important to study. Figure 9 shows the variation of peak responsivity-bandwidth product as a function of Sn composition. This variation almost follows the variation in peak responsivity.

Except very low bias, significant value of the product can be obtained on suitable choice of Sn-content. Study has been extended for some other values of bias voltages also and the values of bandwidth (BW), peak responsivity (R_p), and their product (R_p-BW) are summarized in Table 3 for quick reference.

6. Conclusions

Performance of Gr-IV based interband QWIP with a direct band gap $Ge_{1-x}Sn_x$ active layer is analyzed in detail by developing a theoretical model for the device. Concerning fabrication of such devices, strain balanced structure is considered in this analysis. Effect of strain on energy bands in presence of Sn into GeSn and SiGeSn alloys and quantum mechanical phenomenon are considered in the model. Variation of transit time limited bandwidth, responsivity and responsivity-bandwidth product of the device are analyzed mainly by varying Sn-composition and bias voltage. Results show that Sn–content (x) and applied bias have important role on the bandwidth and responsivity of the device. Both the bandwidth and responsivity increase with increasing bias in a nonlinear manner.

Small bias is sufficient to obtain significant bandwidth, e.g., 200 GHz can be obtained at a bias of only 0.28 V for Sn content of 17%. Thus, the proposed QWIP is a potential candidate to be used in cheap and commercial CMOS based EPICs which require high speed, as well as low voltage. Peak responsivity of 8.6 mA/W is obtained at a bias of 0.5 V for x = 0.17. It is observed that the responsivity, high value of which is always preferred for QWIP, is not too high as the single quantum well structure is used in this analysis. Bandwidth and responsivity can be increased further by increasing Sn-content but as per the report in Ref. [44], it should be limited to 20% due to intolerable strain.

Actually, prime objective of the authors here is to understand the inside physics of a Gr-IV based direct band gap QWIP and to obtain the nature of variation of its performance parameters with Sn-composition in GeSn alloy. So, the single QW is considered in the analysis. However, responsivity can be improved by employing multiple quantum well structure. But in that case, transit time will also increase which will reduce the bandwidth of the device. Resonant cavity enhanced structure can be used to overcome this trade-off and this may be studied further. The analysis presented here may be helpful to obtain suitable design for Gr-IV-based high performance QWIP depending on the areas of application of the device, before its fabrication.

Acknowledgements

This work is partly supported by the Center of Excellence in Renewable Energy, project under MHRD, Govt. of India (F. No. 5-6/2013-TS-VII) at Indian Institute of Technology (Indian School of Mines) Dhanbad, India.

References

[1] V. Gueriaux, et al., Quantum well infrared photodetectors:present and future, Opt. Eng. 50 (2011) 061013.
[2] A. Rogalski, Infrared detectors: an overview, Infrared Phys. Technol. 43 (2002) 187–210.
[3] C. Downs, T.E. Vandervelde, Progress in infrared photodetectors since 2000, Sensors 13 (2013) 5054–5098.
[4] K.W. Ang, et al., Silicon photonics technologies for monolithic electronic-photonic integrated circuit (EPIC) applications: current progress and future outlook, Proc. of IEEE International Electron Devices Meeting (IEDM) (2009) 1–4.
[5] G.Q. Lo, et al., Silicon photonics technologies for monolithic electronic-photonic integrated circuit, ECS Trans. 28 (2010) 3–11.
[6] R. Soref, Mid-infrared photonics in silicon and germanium, Nat. Photonics 4 (2010) 495–497.
[7] G. Roelkens, et al., Silicon-based photonic integration beyond the telecommunication wavelength range, IEEE J. Sel. Top. Quantum Electr. 20 (July/August (4)) (2014) 394–404.
[8] C.H.L. Goodman, Direct-gap group IV semiconductors based on tin, IEEE Proc. I: Solid State and Electron Devices 129 (1982) 189–192.
[9] R.A. Soref, C.H. Perry, Predicted bandgap of the new semiconductor SiGeSn, J. Appl. Phys. 539 (1991) 539, http://dx.doi.org/10.1063/1.347704.
[10] J. Kouvetakis, J. Menedez, A.V.G. Chizmeshya, Tin based group IV semiconductors: new platforms for opto and micro electronics and silicon, Annu. Rev. Mater. Res. 36 (2006) 497–554.
[11] A. Gassenq, et al., GeSn/Ge heterostructure short-wave infrared photodetectors on silicon, Opt. Express 20 (2012) 27297–27303.
[12] J. Werner, et al., Germanium–tin p-i-n photodetecors integrated on integrated on silicon grown by molecular beam epitaxy, Appl. Phys. Lett. 98 (6) (2011), 061108.
[13] J. Zheng, et al., GeSn p i n photodetectors with GeSn layer grown by magnetron sputtering epitaxy, Appl. Phys. Lett. 108 (3) (2016), 033503.
[14] E. Daukes, K. Kawaguchi, J. Zhang, Strain-balanced criteria for multiple quantum well structures and its signature in X-ray rocking curves, Crystal Growth Des. 2 (2002) 287–292.
[15] P. Pareek, M.K. Das, Theoretical analysis of direct transition in SiGeSn/GeSnstrain balanced QWIP, Opt. Quantum Electr. 228 (2016) 1–11.
[16] K.M.S.V. Bandara, B.F. Levine, R.E. Leibenguth, M.T. Asom, Optical and transport properties of single quantum well infrared photodetectors, J. Appl. Phys. 74 (1993) 1826.
[17] V. Ryzhii, High-frequency performance of single quantum well infrared photodetectors at high power densities, IEEE Trans. Electron Devices 45 (8) (1998) 1797–1803.
[18] V. Ryzhii, Impact of transit time and capture effects on high-frequency performance of multiple quantum well infrared photodetectors, IEEE Trans. Electron Devices 45 (1) (1998) 293–298.
[19] B.F. Levine, Quantum well infrared photodetectors, J. Appl. Phys 74 (1993) R1.
[20] N. Yahyaoui, N. Sfina, J.-L. Lazzari, A. Bournel, M. Said, Band engineering and absorption spectra in compressively strained Ge0.92Sn0.08/Ge (001) double quantum well for infrared photodetection, Phys. Status Solidi C 11 (2014) 1561–1565.
[21] N. Yahyaoui, et al., Performance evaluation of high-detectivity p-i-n infrared photodetector based on compressively-strained $Ge_{0.964}Sn_{0.036}$/Ge multiple quantum wells by quantum modeling, Semicond. Sci. Technol. 30 (085016) (2015) 8.
[22] R. Soref, Emerging SiGeSn integrated-photonics technology, in: 2016 IEEE Photonics Society Summer Topical Meeting Series (SUM), CA, 2016, pp. 100–101, http://dx.doi.org/10.1109/PHOSST.2016.7548747.
[23] G.E. Chang, S.W. Chang, S.L. Chuang, Strain-balanced Ge_zSn_{1-z}-Si_xGe_ySn1-x-y multiple-quantum-well lasers, IEEE J. Quantum Electr. 46 (2010) 1813–1820.
[24] Seyed Amir Ghetmiri, et al., Study of a SiGeSn/GeSn/SiGeSn structure toward direct bandgap type-I quantum well for all group-IV optoelectronics, Opt. Lett. 42 (3) (2017) 387–390.

www.czasopisma.pan.pl PAN www.journals.pan.pl
POLSKA AKADEMIA NAUK

[25] Wei Dou, et al., Structural and optical characteristics of GeSn quantum wells for silicon-based mid-infrared optoelectronic applications, J. Electr. Mater. 45 (12) (2016) 6265–6272, http://dx.doi.org/10.1007/s11664-016-5031-2.

[26] N.R. Das, M.J. Deen, Calculating the photocurrent and transit-time-limited bandwidth of a heterostructure p-i-n photo-detector, IEEE J. Quantum Electr. 37 (12) (2001) 1574–1587.

[27] S.M. Sze, Physics of Semiconductor Devices, Wiley-Interscience, USA, 1969.

[28] S.D. Gunapala, D.R. Rhiger, C. Jagadish, Advances in Infrared Photodetectors, vol. 84, 1st Edition, 2011.

[29] H.M. Khalil, N. Balkan, Carrier trapping and escape times in p-i-n GaInNAs MQW structures, Nanoscale Res. Lett. 9 (2014) 1–4.

[30] C.G. Van de Walle, Band lineups and deformation potentials in the model-solid theory, Phys. Rev. B 39 (1989) 1871–1883.

[31] M.K. Das, N.R. Das, Calculating the responsivity of a resonant cavity enhanced $Si_{1-x}Ge_x$/Si multiple quantum well photodetector, J. Appl. Phys. 105 (2009) 1–8, 093118.

[32] G. Zhou, P. Runge, Modeling of multiple-quantum-well p-i-n photodiodes, IEEE J. Quantum Electr. 50 (April (4)) (2014) 220–227.

[33] J. Mathews, Investigation of Light Absorption and Emission in Ge and GeSn Films Grown on Si Substrates, Arizona State University, 2011, PhD Dissertation.

[34] L. Thibaudeau, P. Bois, J.Y. Duboz, A self consistent model for quantum well infrared photodetectors, J. Appl. Phys. 79 (1996) 446, http://dx.doi.org/10.1063/1.362712.

[35] M.K. Das, N.R. Das, Effect of Ge composition on the frequency response of a Si/Si1-yGey P-i-N photodetctor, Opt. Eng. 45 (12) (2006) 1–6, 124001.

[36] J.M. Senior, Optical Fiber Communication, Prentice Hall, London, 1985.

[37] P. Bhattacharya, Semiconductor Optoelectronic Devices, Pearson Education Inc., New Jersey, 1994.

[38] S.W. Chang, S.L. Chuang, Theory of optical gain of Ge-$Si_xGe_ySn_{1-x-y}$ quantum-well lasers, IEEE J. Quantum Electr. 43 (March (3)) (2007) 249–256.

[39] N. Yahyaoui, N. Sfina, J.L. Lazzari, A. Bournel, M. Said, Wave function engineering and absorption spectra in $Si_{0.16}Ge_{0.84}/Ge_{0.94}Sn_{0.06}/Si_{0.16}Ge_{0.84}$ strained on relaxed $Si_{0.10}Ge_{0.90}$ type I quantum well, J. Appl. Phys. 115 (2014) 1–9, 033109.

[40] E. Kasper, et al., Growth of silicon based germanium tin alloys, Thin Solid Films 520 (2012) 3195–3200.

[41] R. Chen, et al., Material characterization of high Sn-content, compressively-strained GeSn epitaxial films after rapid thermal processing, J. Crystal Growth 365 (2013) 29–34.

[42] M. Oehme, et al., GeSn/Ge multiquantum well photodetectors on Si substrates, Opt. Lett. 39 (2014) 4711–4714.

[43] H. Cong, et al., Silicon based GeSn p-i-n photodetector for SWIR detection, IEEE Photonics J. 8 (October (5)) (2016) 1–6.

[44] H.S. Mączko, R. Kudrawiec, M. Gladysiewicz, Material gain engineering in GeSn/Ge quantum wells integrated with an Si platform, Sci. Rep. 6 (2016), http://dx.doi.org/10.1038/srep34082.

[45] M. Oehme, et al., GeSn-on-Si normal incidence photodetectors with bandwidths more than 40 GHz, Opt. Express 22 (2014) 839–846.

[46] P. Rauter, et al., SiGe quantum well infrared photodetectors on pseudosubstrate, Appl. Phys. Lett. 94 (081115) (2009), http://dx.doi.org/10.1063/1.3089817.

[47] Chia-Ho Tsai, Guo-En Chang, GeSn/Ge quantum well photodetectors for short-wave infrared photodetection: experiments and modeling, 16 May 2017, in: Proc. SPIE 10231, Optical Sensors, 102310J, 2017, http://dx.doi.org/10.1117/12.2265185.

[48] G.E. Chang, et al., Design and modeling of GeSn-based heterojunction phototransistors for communication applications, IEEE J. Sel. Top. Quantum Electr. 22 (Nov.-Dec) (2016) 425–433.